Rapid Generation of Structured Physical Phantoms for Mammography and Digital Breast Tomosynthesis

Lynda Ikejimba[✉], Christian Graff, and Stephen Glick

Division of Imaging, Diagnostics, and Software Reliability,
OSEL/CDRH/FDA, Silver Spring, USA
{Lynda.Ikejimba,Christian.Graff,
Stephen.Glick}@fda.hhs.gov

Abstract. Nonuniform phantoms are needed in order to fully characterize the impact of anatomical structures on system performance in mammography and digital breast tomosynthesis (DBT). In this work, a new type of textured physical phantom is presented, compatible for use in both 2D and 3D applications. The breast phantom was first modeled analytically, and then fabricated using inkjet printing onto parchment paper and slide transparencies. A radiographic ink solution was synthesized with 350 mg/mL iohexol and pigmented ink. The effective linear attenuation coefficient (μ_{eff}) of the parchment paper alone (0.078 ± 0.003 mm^{-1}) was found to be very close to that of a 70 % adipose, 30 % fibroglandular tissue mixture (0.078 ± 0.004 mm^{-1}). The μeff of the parchment paper with iodine (0.010 ± 0.005 mm^{-1}) was close to that of 100 % fibroglandular tissue (0.11 ± 0.004 mm^{-1}). This new parchment and iodine phantom has strong potential for use in imaging studies.

Keywords: Breast phantom · Anthropomorphic · Iodine · Linear attenuation

1 Introduction

Physical breast phantoms remain a cornerstone for the effective evaluation and quality control (QC) of clinical imaging systems, such as full field digital mammography (FFDM) and digital breast tomosynthesis (DBT). In mammography, a planar radiograph is taken, and the resulting 2D image contains superposing tissue from various depths in the breast. However, the standard evaluation phantoms consist of a layer of inserts against a uniform backgrounds, which do not reflect the true structure of the breast [1, 2]. In DBT, a series of projection radiographs are acquired and reconstructed to create a 3D volume. Since DBT uses a limited number of angular projections, the resulting volume is undersampled and suffers from out of plane artifacts. Additionally, because the aforementioned phantoms were originally designed for use with 2D systems, they may not capture aspects of 3D imaging that may be of interest, such as the axial spread function or partial volume artifacts. An important component of measuring performance could then incorporate the extent to which out-of-plane structures are

suppressed. For these reasons, it is of great interest to use a structured 3D phantom in both FFDM and DBT evaluation.

Work has been done to create physical breast phantoms with nonuniform texture. Such phantoms may be based on patient histology [3], consist of acrylic spheres [4], or contain other complex arrangements of glandular and adipose tissues [5, 6] and fabrication using additive manufacturing techniques [6]. Typically, these phantoms also follow the same power law properties of the breast. However, some drawbacks to these phantoms include resolution limitations, cost, and the time to produce each one. In this work, we develop a new type of 3D phantom that can model random anatomy and can be quickly fabricated from inkjet printing.

2   Materials and Methods

2.1   Virtual Modeling of Breast Phantom

The in silico breast phantom was procedurally generated using a recently described model [7] developed in our group. The procedure can be summarized as follows: An anthropomorphic uncompressed breast shape was created based on a series of parameters controlling breast volume and surface curvature. A skin layer and nipple were generated to cover the surface of the breast shape. The interior of the breast was segmented into fat regions and glandular compartments based on a random Voronoi segmentation. Within each glandular compartment a ductal tree with terminal duct lobular units were generated. Cooper's ligaments were created using a network of random Perlin-noise perturbed surfaces. Perlin noise interpolates randomly generated gradient directions across multiple length scales. This type of noise is commonly used to procedurally generate textures reminiscent of the randomness found in nature. In this work we have created fat lobules with random shapes by perturbing the surface of a base spheroid with Perlin noise tuned to qualitatively resemble fat lobule surface variability observed in vivo. A vascular tree was grown using random branching structures emanating from a muscle layer at the base of the breast phantom. This model was digitized with voxels of 120 μm, which was adequate for the present application. To model compression, a tetrahedral mesh was generated, with each element assigned either glandular or fat elastic properties based on the voxels contained within the element. A linear elasticity finite element method was used to model compression of the breast to a thickness of 30 mm. For the present study, this thickness was selected to represent a smaller breast, but in practice a breast of any thickness could be created.

All breast surfaces are defined analytically so there is no inherent limitation to voxel size or total breast volume. For efficient computation it is necessary to store the entire phantom in memory during generation, which imposes a practical limit on the total number of voxels in the phantom. For an average size breast, 40 micron voxels are achievable on a computer with at least 8 GB of RAM. The computational time scales with the number of voxels, so time constraints can also impose practical limits on voxel or breast size.

2.2   Printing of Physical Phantom

The virtual phantoms were realized through inkjet printing with radiopaque ink onto a thin material base. The radiopaque ink was created by mixing 350 mg/mL iohexol (Omnipaque, GE Healthcare, Princeton, NJ) with pigmented ink (InkThrift, Vermont PhotoInkjet) in a solution of 25 % iohexol and 75 % ink. The solution was inserted via syringe into refillable inkjet cartridges. Using this solution, the virtual phantom was then printed slice by slice at the nominal resolution of 120 µm or 210 dpi. The phantom was printed onto several types of material. The first was 70 µm thick parchment paper with a silicone coating. The second was 120 µm thick slide transparency (C-Line). The final was a 100 µm thick "organic" paper. The background material would serve as the adipose-only component of the breast, while the glandular components are overlaid with the printed ink. Since each printed sheet corresponds anatomy at a different depth of the virtual breast, the composite physical phantom can be used in 3D imaging modalities. Fiducial markers were placed on each slice of the virtual model to assist with aligning the pages.

Because each slice of the phantom is printed on a single sheet of paper, the final height of the printed stack can be affected by the thickness of the paper. For example, the 120 µm paper will yield a stack closer to 30 mm. However, for thinner paper the final stack height may be slightly less than 30 mm.

2.3   Image Acquisition

For validation of the materials used, the attenuation properties of the phantom materials were compared with those from six tissue equivalent chips of known glandular density ranging from 0 % glandularity (100 % adipose) to 100 % glandularity (CIRS, Norfolk, VA). Phantoms images were acquired on a clinical mammography system (Hologic Lorad Selenia, Bedford, MA). A target/filter combination of molybdenum/molybdenum was used to examine the material properties under typical mammographic beams. The source to imager distance was 660 mm, using an a-Se direct detection imager with 70 µm pixel pitch. Images were processed only for gain map correction.

The effective linear attenuation coefficient μ_{eff} was calculated from Beer's law. To obtain the incident exposure, an open field image was acquired without the phantom. In addition, to determine the dark field offset an acquisition was made with zero exposure onto the detector; this offset was then used to correct both the phantom and open field images prior to numerical calculations. Finally, the effect of scatter was also measured from the air gap method. Images of the phantom are presented in Fig. 1 as (a) a slice through the binary digital model, (b) a picture of the physical realization, with a side view of the stack thickness inset, and (c) a radiograph with Mo/Mo at 28 kVp. For demonstration purposes, the images in Fig. 1(b), (c) represent only a subset of the stack, with duplicate prints of some slices to enhance visibility.

Fig. 1. Fabrication of physical phantom. The phantom was (a) designed as a virtual model, (b) realized through printing and (c) x-rayed on a mammographic system.

3   Results and Discussion

The effective linear attenuation coefficient was measured for the tissue chips of known glandular fraction, and data are provided in Fig. 2. Results were found to be in good agreement with published data [6]. At 28 kVp, the attenuation coefficients of the chips were plotted against their percent glandular density. The relationship was determined to be linear, and the equation of fit provided a correspondence between the effective linear attenuation coefficient and an approximate glandular fraction, for a given beam condition. Error bars on the estimates are from the pixel variance and slight variability in sample thickness. This linear mapping was then used to determine an equivalent glandular density for the parchment paper, transparency slides, and organic paper. Scatter was measured through the air gap method, and determined to have a small effect (<7 %) on the calculated attenuation values.

Results are plotted in Fig. 3 of the μ_{eff} and estimated glandular density for the six tissue equivalent chips and sheets of material, obtained with Mo/Mo at 28 kVp. For a given material sample, the μ_{eff} is given on the left axis and the equivalent percent glandular density, derived from the linear regression equation, is give on the right axis. The column labeled "100 % G" denotes the chip of 100 % glandular density, "70 % G" the 70 % glandular density, and so on. The column labeled "BR12" corresponds to a sample of the BR12 consistency testing material, equivalent to 47 % glandular/53 % adipose. An estimated glandular density below zero indicates the material is less dense than adipose tissue. The results show that the μ_{eff} of the parchment paper alone, 0.078 ± 0.003 mm^{-1}, was very close to that of the 30 % glandular chip, 0.078 ± 0.004 mm^{-1}. For the fibroglandular component, the μ_{eff} of the parchment with iodine was approximately 0.010 ± 0.005 mm^{-1}, compared to the 100 % glandular chip with 0.11 ± 0.004 mm^{-1}. The slide transparency was equivalent to about 100 % glandularity on its own, and was much higher with the addition of iodine. Similarly, the approximate glandular density of the paper alone exceeded 100 %, and with iodine was almost 175 %.
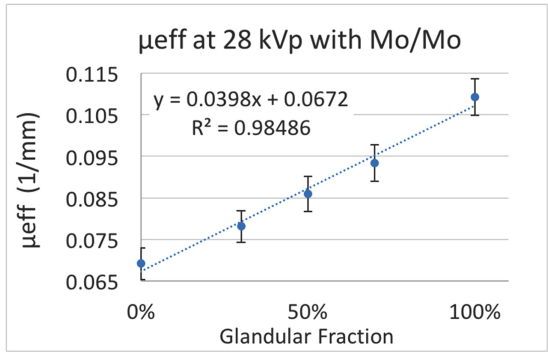
Fig. 2. Mapping of μ_{eff}. The μ_{eff} was computed for each material at a specific tube voltage. Linear regression was applied to determine the relationship between the x-ray attenuation coefficients and the percent glandularity of the materials.
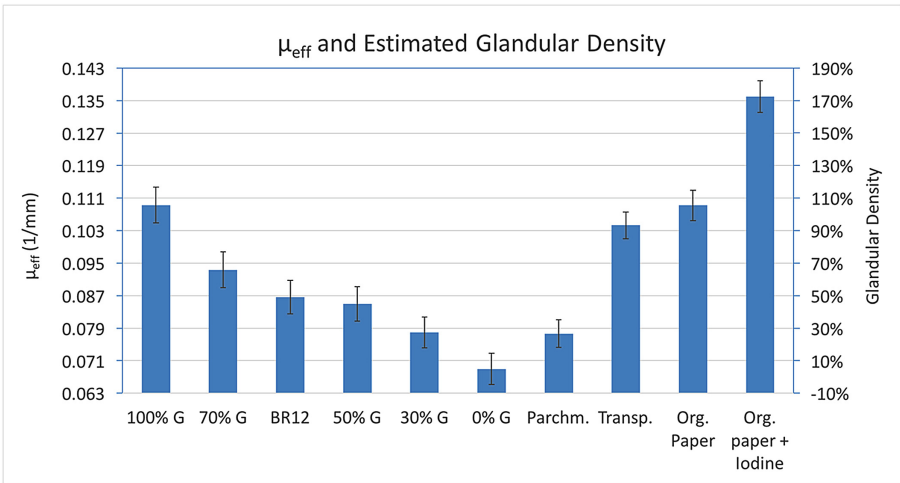
Fig. 3. μ_{eff} and glandular density of sheet materials and tissue chips. The linear attenuation coefficients of the phantom materials were compared with those of known glandular density.

Phantom printing is a promising area of active research, particularly with the use of additive manufacturing techniques. However, current additive manufacturing techniques have limited feasibility due to the high cost of the printing machine and inks, along with a small selection of desirable materials. The method presented in this study, however, uses readily available materials to produce a cheap and fully customizable 3D structured phantom with realistic material properties.

The results of the analysis showed that the parchment paper and iodine ink can be used to create a phantom with similar x-ray properties as breast tissue glandular tissue, under the beam conditions considered. Because the phantom is not limited to two materials, it is possible to print other anatomical features of interest, such as lesions or

microcalcifications (MC). Additionally, because the model resolution is arbitrary, a smaller voxel size may be selected to better resolve microcalcifications smaller than 120 μm. Once created, these features can be easily inserted into and removed from the phantom by printing the mass or MC over multiple sheets and simply replacing select slices within the original phantom. The phantom can also be modeled with blood vessels, thus the modeling of iodine uptake through the breast arterial system would also be possible. While an analytical virtual phantom is used here, another benefit of the technique is that it is not limited to such models and can readily be applied with any type of voxelized phantom. The realism of the virtual model was not the primary focus of this work, and its appearance was not evaluated by radiologists. However, the present approach provides a method to print any virtual breast model using tissue equivalent materials.

4   Conclusions

Structured phantoms are necessary for evaluating 2D and 3D breast imaging systems. Existing phantoms can be expensive, time consuming to create, or limited in their anatomical realizations. In this work we demonstrated a unique technique for printing 3D physical breast phantoms with a radiographic ink and parchment paper. The x-ray attenuation properties of the ink and parchment allowed us to print glandular structures directly onto an adipose-like background. This method enables for the cheap, rapid creation of breast tissue-equivalent phantoms with great diversity.

References

1. McLelland, R., Hendrick, R.E., Zinninger, M.D., Wilcox, P.A.: The American college of radiology mammography accreditation program. AJR Am. J. Roentgenol. **157**, 473–479 (1991)
2. Thijssen, M.A.O., Bijkerk, K.R., Van der Burght, R.J.M.: Manual contrast-detail phantom Artinis CDMAM type 3.4. University Medical Center Nijmegen, Department of Radiology, The Netherlands, Utilisation Manual 2006 (2007)
3. Carton, A.K., Bakic, P., Ullberg, C., Derand, H., Maidment, A.D.: Development of a physical 3D anthropomorphic breast phantom. Med. Phys. **38**, 891–896 (2011)
4. Gang, G., Tward, D., Lee, J., Siewerdsen, J.: Anatomical background and generalized detectability in tomosynthesis and cone-beam CT. Med. Phys. **37**, 1948–1965 (2010)
5. Freed, M., Badal, A., Jennings, R.J., de las Heras, H., Myers, K.J., Badano, A.: X-ray properties of an anthropomorphic breast phantom for MRI and x-ray imaging. Phys. Med. Biol. **56**, 3513 (2011)
6. Kiarashi, N., Nolte, A.C., Sturgeon, G.M., Segars, W.P., Ghate, S.V., Nolte, L.W., Samei, E., Lo, J.Y.: Development of realistic physical breast phantoms matched to virtual breast phantoms based on human subject data. Med. Phys. **42**, 4116–4126 (2015)
7. Graff, C.G.: A new open-source multi-modality digital breast phantom. In: Medical Imaging 2016: Physics of Medical Imaging. Proceedings of SPIE, vol. 9783 (2016). doi:10.1117/12.2216312